Evapotranspiration variations in the Yangtze River Basin from multi-satellite remote sensing data

Xiaojuan Tian and Shuanggen Jin

ABSTRACT

Evapotranspiration (ET) variations in the Yangtze River Basin (YRB) are influenced by environmental and climate changes related to planting of crops, forest vegetation, water use and other human activities. However, it is difficult to measure ET variations and analyse influencing factors in the YRB due to lack of in-situ measurements. In the present study, the ET variations were estimated and investigated in the whole, the upper, middle and lower reaches of the YRB using the Gravity Recovery and Climate Experiment (GRACE), optical remote sensing data and hydrological models based on a water balance method, which was validated by MODerate Resolution Imaging Spectroradiometer (MODIS) observations and models. Furthermore, GRACE-ET verified the drought events in 2006 and 2011. The long-term variation rate of GRACE-ET is 0.79 mm/yr. The spatial distribution of seasonal ET variations indicates that ET is highest in summer and lowest in autumn-winter. It also shows that the completion of the Three Gorges Project has certainly increased ET. Precipitation and temperature have the largest impact on the ET variations; radiation and soil moisture have moderate effects. ET variations in the middle and lower reaches are greatly affected by precipitation, and temperature plays a more important role in the upper YRB reaches.

Key words | climate change, evapotranspiration, GRACE, Yangtze River Basin (YRB)

Xiaojuan Tian
Shuanggen Jin (corresponding author)
Shanghai Astronomical Observatory,
Chinese Academy of Sciences,
Shanghai 200030,
China
E-mail: *sgjin@shao.ac.cn*;
sg.jin@yahoo.com

Xiaojuan Tian
University of Chinese Academy of Sciences,
Beijing 100049,
China

Shuanggen Jin
School of Remote Sensing and Geomatics Engineering,
Nanjing University of Information Science and Technology,
Nanjing 210044,
China

INTRODUCTION

The Yangtze River Basin (YRB) is the third longest river in the world, and only the Amazon and Congo rivers have larger water storage capacity. The YRB is the largest river basin in China, where the population is dense and the economy rich, and also an important agricultural production base (Xu *et al.* 2009). However, the YRB is located in the eastern part of the Eurasian continent and so is subject to the impact of the monsoon, and the vapour transportation system is complex and changeable, resulting in complicated hydrological conditions in the basin, which makes it prone to drought and flooding (Hu 1997). Evapotranspiration (ET) is an important part of the water cycle, through which most of the surface precipitation returns to the atmosphere, thus connecting hydrological, atmospheric and ecological components (Najibi & Jin 2013; Bai *et al.* 2017). Therefore, a long-term sequence estimation of ET variations would be beneficial to understanding of the dynamic variations in the terrestrial water cycle and energy flux. The effective space-time monitoring of ET and analysis of its influencing factors are of significance for water resources management, crop planting, water requirement assessment, drought and flood defence in the YRB (Wang *et al.* 2016). Some studies have shown that influencing factors on ET were very complex (Yang *et al.* 2010). In particular, the YRB (Figure 1) stretches across the three belts of China with complex and changeable topography, numerous tributary lakes, and significant difference in precipitation between the east and the west. Furthermore, it is sensitive

doi: 10.2166/wcc.2018.104

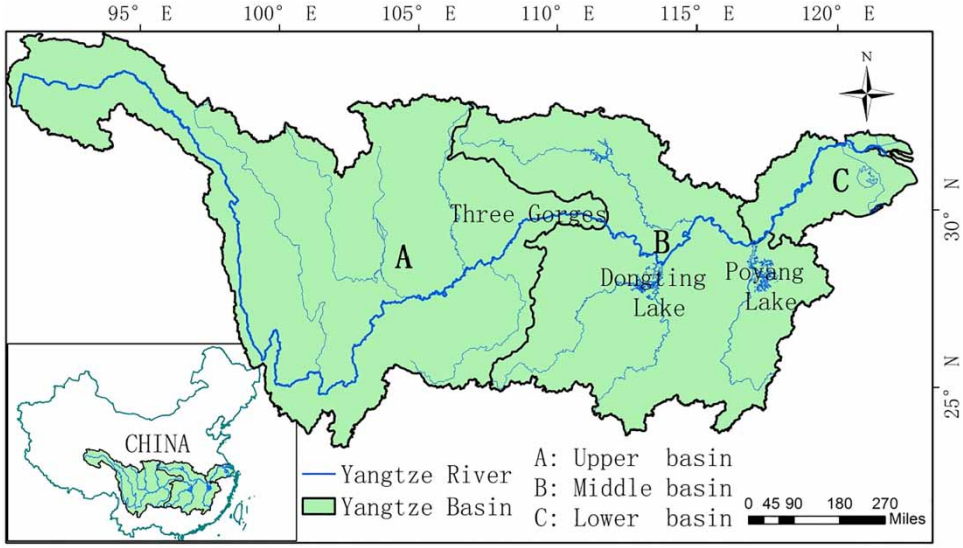

Figure 1 | Map of the Yangtze River Basin.

to global environmental change, ecologically fragile and affected by frequent human activities and numerous dams (Verstraeten *et al.* 2008), so it is important to investigate the detailed regional characteristics of ET variations in YRB as well as its effect factors.

ET has been estimated from traditional field measurements, empirical formulas, algorithms and satellite remote sensing observations as well as terrestrial hydrological models and data assimilation methods, but it still has large uncertainty due to limited in-situ observations and high costs, e.g. lysimeter, scintillation counter (Monteith 1965). Traditional field measurement methods do not need to add complex algorithms and data processing, but require a great deal of manpower and material resources to maintain the measuring tools, and also it is difficult to realize long-term sequences of ET measurement over large areas. Along with the development of the empirical formula methods to estimate ET, based on the physical characteristics of the natural ground, e.g. the Penman–Monteith (PM) method developed from the Penman method (Antonopoulos & Antonopoulos 2017), empirical algorithms need to input some surface physical quantities, such as wind speed, vapour pressure and humidity, which increases the difficulty of estimating ET for large areas and long-term sequences. Therefore, empirical algorithms are generally applied to ET estimation at a small scale (Baik & Choi 2015). Optical satellite remote sensing data also enhances the estimation of ET, and has been widely used with the help of empirical algorithms. The thermal infrared band of remote sensing satellites can monitor ground surface radiation, thus realizing the energy balance equation (Minacapilli *et al.* 2009). The surface radiation is combined with the near infrared and visible bands of remote sensing satellites to monitor vegetation cover, and the estimation of ET is realized by the empirical algorithms (Zhang & Jin 2016). The remote sensing data greatly improve the efficiency of ET estimation, which is beneficial to studies of hydrological and environmental climate changes globally. However, because optical remote sensing is greatly affected by weather conditions and cloud cover, the study of a basin needs multiple images to be spliced, increasing the difficulty of continuous, whole area observation. Moreover, the remote sensing data are based on empirical algorithms, in which the coupling conditions of physical quantities are regional, and different surface environments require different model parameters. Global Positioning System (GPS) observations have been used to estimate the ET variations in the Mississippi River Basin; this method is novel and sensitive to large-scale ranges, but it needs more dense and continuous GPS observation stations to work optimally (Zhang & Jin 2016).

The GRACE (Gravity Recovery and Climate Experiment) gravity satellite, launched in 2002, can estimate

variations in water storage, which can directly reflect dynamic changes on the Earth without meteorological data and experience algorithms (Tapley *et al.* 2004). Determination of the Earth's gravitational field is not influenced by weather conditions or cloud cover. It has been widely used in global climate and hydrology, such as monitoring glacier and snow melting, drought and flood, and groundwater changes (Jin & Zou 2015; Jin *et al.* 2016a, 2016b). GRACE has also been applied to the study of ET, but few studies have been done. Combining optical remote sensing data and hydrological models, with a water balance method, GRACE-derived ET will provide a new opportunity to monitor ET variations and analyse the influencing factors.

This study aims to: (1) estimate and compare long sequence ET changes in the whole YRB as well as the upper, middle and lower reaches from August 2002 to August 2016 by GRACE; (2) investigate the interannual variations, seasonal variations and long-term variations of ET in YRB from GRACE through the water balance equation together with Moderate Resolution Imaging Spectroradiometer (MODIS) remote sensing data and hydrological models, and to discuss its spatial distribution; and (3) analyse in detail the influencing factors (precipitation, soil moisture, surface temperature and solar radiation) on ET variations in the whole, the upper, middle and lower reaches of YRB.

DATA AND METHODS

Study area

The Yangtze River (Figure 1) is the third longest river in the world, about 6,300 km long, and the basin area is 1.8×10^6 km^2, stretching across the three belts of China. The YRB is divided into the upper, middle and lower reaches from west to east. The topography gradually decreases from west to east, and the landforms are diverse. The western plateau belongs to the cold climate zone, and most of the basin is the East Asian or South Asian monsoon climate zone, with four different seasons, controlled by the Asian monsoon (Zhang *et al.* 2008). The upper basin of the Yangtze River originates from the Tuotuo River on the western Tibetan Plateau and stretches to Yichang. With mountain ranges as the main terrain, there is a significant vertical climatic spectrum, and hydropower resources are abundant. The Three Gorges Dam, the world's largest dam, is situated on the Yangtze River. From Yichang to Hukou, comprises the middle basin, with scattered alluvial plains, low hills and lakes, with an altitude below 200 m. In the middle reaches, the Jianghan Plain, with a large population, is an important agricultural production base in central China. The lower reaches of the Yangtze River stretch from Hukou to the Yangtze River Estuary in Shanghai on the Yangtze River Delta Plain, with an altitude of only 2–5 m are very sensitive to oceanic storms. It is an important economic development zone in China, with a large population density and a highly developed economy. Although the runoff of the YRB was mainly supplied by precipitation, more than half of precipitation evaporated, so ET is one of most important elements of water balance in the YRB.

Observation data

GRACE

The GRACE satellite, launched in 2002, is a cooperative project between the National Aeronautics and Space Administration (NASA) and the German Aerospace Center. GRACE can estimate Earth's time-variable gravity field with monthly temporal resolution and spatial resolution of hundreds of kilometres. The GRACE gravity products for a total of 156 months from April 2002 to August 2016 are used in this paper (data missing in June and July 2002; June 2003; January and June 2011; May and October 2012; March, August and September 2013; February, July and December 2014; June, October and November 2015; April 2016). These products are provided by Center for Space Research of the University of Texas at Austin. The highest order of Stokes coefficients of spherical harmonic function for products of RL05 GSM data is 60. The anomalous gravity field was deducted from the multi-year mean gravity field. The impacts of redistribution of atmospheric and oceanic mass, as well as the effects of tides have been calculated by means of models, and therefore variations in the remaining Earth's gravity field are mainly caused by changes in land water mass.

Because of the existence of north–south striping noise in spherical harmonic coefficients, and errors in high-order Stoke coefficients (Wahr *et al.* 1998), spatial filtering is necessary before the spherical harmonic coefficients are estimated as the mass change of land. In this study, the P5M6 decorrelation filter was used (Swenson & Wahr 2006). For example, for the coefficients of the harmonic coefficients ranked sixth-order and above (e.g. Cn,6, $n = 6$, 7, …, 60), we carried out the least squares 5-item processing, the so-called P5M6, to perform the Destripe TM Data. Then the Gauss filter (Jekeli 1981) with an average radius of 400 km was used to remove the rest of the noise. The monthly variations of gravity field were used to calculate the land equivalent water height of $1^\circ \times 1^\circ$ grid. Because of the great uncertainty of the second-order coefficients, the C_{20} term spherical harmonic coefficients were replaced by the satellite laser ranging of higher quality (Jin *et al.* 2011), and the degree-1 coefficients were provided by Swenson & Wahr (2006). The impact of post glacial rebound in YRB is small and negligible (Peltier 2004).

Precipitation data

As precipitation is the only source of water input in the land water cycle, it is particularly important in ET estimation. At the global scale, traditional rainfall data are calculated by means of the rain gauge network, but regional precipitation measurements are difficult to achieve. Remote sensing satellites can provide global coverage of precipitation. In this study, we used the precipitation data from TRMM (Tropical Rainfall Measuring Mission), a tropical rainfall measuring mission jointly developed by NASA and Japan's National Space Development Agency. The TRMM satellite was launched at the space centre in Tanegashima, Japan on 28 November 1997, with a track height of 350 km; this satellite monitors the precipitation conditions of the low and middle latitudes of the earth (50°N–50°S). Here the grid rainfall data of TRMM-3B43 from August 2002 to August 2016 were used with the spatial resolution of $0.25^\circ \times 0.25^\circ$, and the products were converted from 3 hours data to data with temporal resolution of 1 month. In order to keep consistent with GRACE data, the rainfall variations of $1^\circ \times 1^\circ$ in YRB were obtained by averaging and resampling through the 4×4 window. Another kind of precipitation data used in this paper was from GPCC (Global Precipitation Climatology Centre), which was developed for material selection, quality control and analysis of global land precipitation through the objective interpolation system. It was based on 85,000 rainfall measurement stations worldwide. The products were from August 2002 to August 2016 with a spatial resolution of $1^\circ \times 1^\circ$ and a time resolution of 1 month.

MODIS data

Remote sensing ET products of MODIS were also used for comparison and analysis. MODIS is carried out by EOS (Earth Observation System) satellites which were launched by NASA. The products are from MOD16 (covering latitude 80°N–60°S, longitude 180°E–180°W), from August 2002 to August 2014 with 1 month temporal resolution and $0.5^\circ \times 0.5^\circ$ spatial resolution. The products are based on the PM method which is an energy balance method (Antonopoulos & Antonopoulos 2017) and is based on surface meteorological parameters such as air temperature, humidity, wind speed and solar radiation.

Hydrological model

The hydrological model of Global Land Data Assimilation System (GLDAS) is a global hydrological model jointly developed by NASA's Goddard Space Flight Center and NOAA's National Centers of Environmental Prediction (NCEP). Surface observation and satellite remote sensing observation data were used to drive four surface process models (Mosaic, Noah, CLM and VIC). The input data of the model were analysis results of precipitation, solar radiation, surface pressure, humidity and surface horizontal wind speed data provided by NCEP, and obtained by remote sensing and by surface observation; output results of the model include soil temperature, soil moisture, ET, runoff, covering the latitudinal and longitudinal ranges of 90°N–60°S and 180°E–180°W. The soil moisture (four layers of soil in 0–2 meters added), surface temperature, solar shortwave radiation and runoff data (used for calculation of the water balance equation – see below) provided by the GLDAS-Noah model from August 2002 to August 2016 were used, ET products of four GLDAS models

(Noah, VIC, CLM and Mosaic) were used for comparison and analysis, of which the spatial resolutions are $1^\circ \times 1^\circ$, and the temporal resolution is 1 month.

Methods

Total water storage (TWS) estimation from GRACE

The land mass variations were estimated by using spherical harmonic coefficients of GRACE gravity field as Wahr *et al.* (1998):

$$\Delta\eta(\theta, \phi) = \frac{a\rho_{ave}}{3\rho_W} \sum_{l=0}^{\infty} \sum_{m=0}^{l} \overline{P_{lm}}(\cos\theta) \frac{2l+1}{1+k_l} (\Delta\overline{C}_{lm} \cos(m\phi) + \Delta\overline{S}_{lm} \sin(m\phi)) \quad (1)$$

where a is the mean equatorial radius of the earth, l and m are respectively the order and the degree of spherical harmonic coefficients, θ is the co-latitude, ϕ is the longitude, C_{lm} and S_{lm} are the gravity field coefficients, $\overline{P}_{lm}(\cos\theta)$ is the normalized Legendre function, ρ_{ave} is the average earth density (5,517 kg/m^3), $\Delta\overline{C}_{lm}$ and $\Delta\overline{S}_{lm}$ are the variations of spherical harmonic coefficients provided by GRACE, k_l is the loading love number, ρ_W is the density of water (1,000 kg/m^3), and the variations of equivalent water thickness $\Delta\eta(\theta, \varphi)$ can be transformed from the density variations in the Earth's surface. Therefore, the water variations in the Earth's surface can be expressed in the form of equivalent water thickness, i.e. the total water storage (TWS).

Long-term change fitting

Since ET shows significant trend, acceleration, seasonal variations with annual and semi-annual periods, it was fitted by the least squares method (Jin & Feng, 2013):

$$ET(t) = a + bt + ct^2 + \sum_{k=1}^{2} d_k \cos(\omega_k t - \varphi_k) + \varepsilon(t) \quad (2)$$

where a is constant item, b is the long-term variation, c is the second order item, d_k is the amplitude, φ_k is the phase, ω_k is the frequency (1 year and 0.5 year), and $\varepsilon(t)$ is the residual item. When k is 1, d_k is annual amplitude and φ_k is annual phase. When k is 2, d_k is semi-annual amplitude and φ_k is semi-annual phase. The 'sum of cos' is a summary of annual term + semi-annual term. The fitting accuracy as sigma was also estimated and is discussed below.

Water balance equation

During the water cycle in a closed system, ET can be estimated based on the water balance equation:

$$\text{ET} = P - R - \partial S/\partial t \quad (3)$$

where ET is the evapotranspiration, P is the precipitation, R is the runoff, $\partial S/\partial t$ is the variation of average water reserves in the basin, S is the variation of water storage inverted by GRACE and t is the time interval of data sampling (here 1 month). Since the TWS estimated by GRACE reserves the precipitation information of the previous month, the monthly variations of average water reserves $\partial S/\partial t$ were obtained by using the month's TWS to subtract the TWS of the previous month. In this paper, the precipitation data were provided by TRMM and GPCC, and the runoff data were provided by GLDAS-Noah hydrological model. All these are grid data with the same temporal resolutions of 1 month, and the same spatial resolution of $1^\circ \times 1^\circ$. The ET calculated by precipitation data from TRMM is called ET-TRMM, and ET-GPCC represents the ET obtained by GPCC precipitation data.

Through the water balance equation, the ET variations in time series and spatial distribution in the whole YRB and the upper, middle and lower YRB reaches were estimated by using the monthly TWS. In this study, TWS from GRACE was used to calculate the variations of ET in YRB from August 2002 to August 2016. ET products from MODIS remote sensing were called ET-MODIS, and ET products exported by GLDAS models were also compared and analysed as shown in Figure 2.

RESULTS AND ANALYSIS

ET estimation

Figure 2 shows monthly mean ET in YRB from August 2002 to August 2016 for four kinds of ET products, including ET deduced from GRACE through the water balance equation,

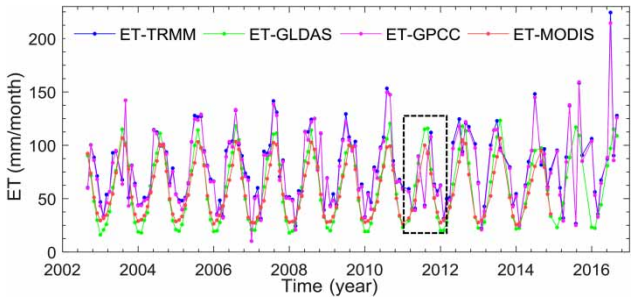

Figure 2 | Comparison of monthly ETs in YRB from August 2002 to August 2016.

output results of GLDAS hydrological model and ET products from remote sensing data. It can be seen that the long-term sequence variations of ET deduced from GRACE are basically consistent with those of ET products from the land hydrological model and remote sensing data. The high(low) values of ET deduced from GRACE are higher than those of ET products from the land hydrological model and remote sensing data, indicating that the method of water balance equation is more accurate in ET estimation. This is consistent with the conclusion of Long *et al.* (2015) that human factors (e.g. water diversion, agricultural irrigation) were not taken into account in ET estimation from remote sensing data and the land hydrological model thus underestimates the ET. In Figure 2, we can see that the variation trends of different ET products throughout 2011, marked out by the black boxes, are unexpectedly consistent, and the ordinary phenomenon that high values of GRACE-derived ET are higher does not appear, indicating the occurrence of severe drought, which verifies the severe drought event that year and is consistent with the conclusion of Zhang *et al.* (2016).

The YRB covers a vast area (1.8×10^6 km^2), with complex and changeable landforms, numerous tributary lakes and significant difference in precipitation between the east and west as well as frequent human activities. Controlled by the monsoon, the precipitation decreases gradually from the east to west. The YRB was divided into the upper, middle and lower reaches (Figure 1) for comparison and analysis. We can see that the overall variation trends in TWS of the total, upper, middle and lower reaches are basically consistent from April 2002 to August 2016, but there are subtle differences. The amplitude in the upper reaches is the largest, second in the middle reaches and the smallest in the lower reaches, which indicates that hydrological variation of the upper reaches is the largest, and that of the lower reaches the smallest. However, the parts marked out by black boxes in Figure 3 show that the TWS variations for the upper reaches in 2006 were lower than in other years, and for the middle and lower reaches in 2011 lower than before and after. The variation in amplitude of TWS in the upper reaches in 2006 should be stronger, but actually it is even less than that of the middle and lower reaches, with the minimum value, which coincides with the drought events in the southwest of China (the upper reaches) in 2006. The amplitude of TWS in the middle reaches in 2011 should be in the middle position, but actually it has the minimum amplitude and the minimum value, which is consistent with the drought events in 2011. In other words, TWS shows consistent results with drought events as described by Zhang *et al.* (2016).

In order to evaluate ET products, we made a correlation analysis of each ET product. As shown in Figure 4, ET from the land hydrological model, remote sensing data and GRACE through the water balance equation has a good correlation, and the correlation coefficients are greater than or equal to 0.84. As deduced from GRACE through the water balance equation, both the correlation coefficients of ET-GRACE-GPCC and ET-GRACE-TRMM reaches 0.99, which indicates that the precipitation data of TRMM and GPCC have great similarity.

The water balance equation shows that precipitation, runoff, ET and water storage change are important links, and each component is closely linked in the water cycle (Equation (3)). As shown in Figure 5, there is 1 month lag between the monthly terrestrial water storage change

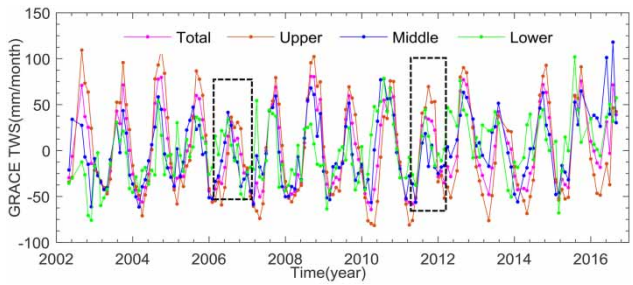

Figure 3 | Comparison of monthly TWS time series variations (mm/month) from GRACE in the whole YRB, the upper, middle and lower reaches from April 2002 to August 2016.

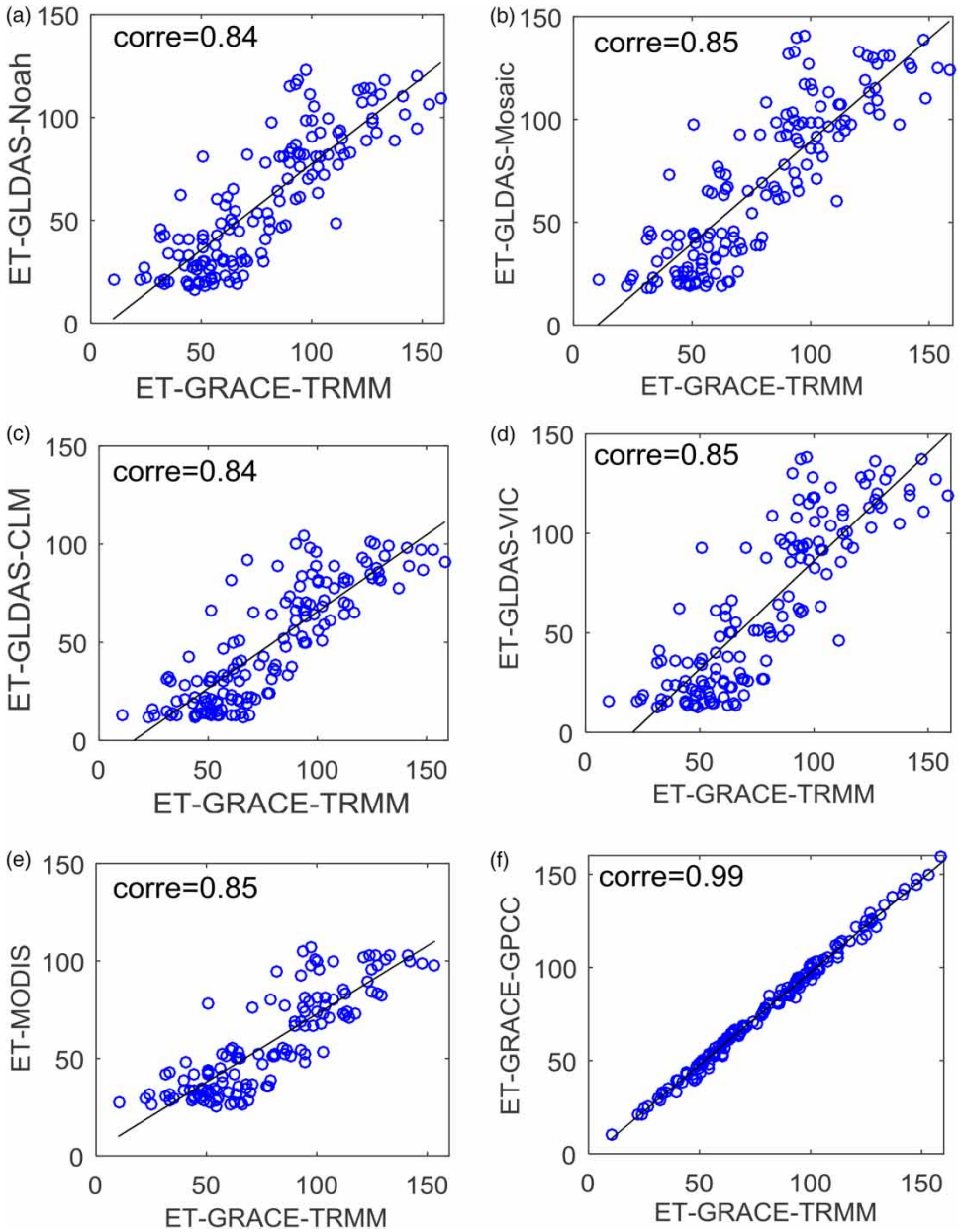

Figure 4 | Scatter plot of ET in the whole YRB deduced from GRACE-TRMM and other calculation results: (a) ET-GLDAS-Noah, (b) ET-GLDAS-Mosaic, (c) ET-GLDAS-CLM, (d) ET-GLDAS-VIC, (e) ET-MODIS, (f) ET-GRACE-GPCC.

inverted by GRACE and precipitation, runoff and ET, the variation trends of precipitation, runoff and ET are basically the same, and the amplitude variation of runoff is mild. Initially that there is great correlation between precipitation and ET, and the amplitudes are basically the same. More detailed analyses are shown below. From Figure 5, some values of ET were higher than those of precipitation. Firstly, some GRACE data are missing, which may bring in errors. Secondly, when using GRACE data, the anomalous gravity field has been extracted from the multi-year mean gravity field, so relative value possibly results in higher ET value by GRACE-based water balance equation than precipitation, but actually it is not higher. Thirdly, when drought occurs, it is normal that the ET

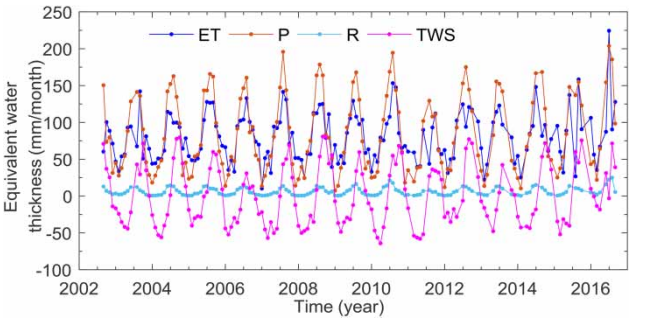

Figure 5 | Comparison of time series variations in monthly mean evapotranspiration (ET), precipitation (P), runoff (R) and terrestrial water storage (TWS) change deduced from GRACE-TRMM in the YRB from August 2002 to August 2016.

value is higher than those of precipitation and the runoff value may be negative at this time.

According to Figure 6, ET products from the water balance equation, land hydrological model and remote sensing data show some common rules: the annual ET amplitude in YRB and the annual variation pattern are basically the same, the annual ET in the upper reaches is the smallest, the annual ET in the middle reaches is the largest, and ET in the lower reaches is slightly less than that in the middle reaches. The annual ET amplitude in the middle and lower reaches are large, which may be related to the dense population and heavy rainfall, but the specific reasons need to be further analysed. The annual ET in the upper reaches is small, which may be due to the small amount of precipitation, relatively lower population, high vegetation coverage and low plateau temperature, which also need to be further analysed. But there are differences in the interannual variation of different ET products: the interannual variations of ET in each region of YRB estimated by the land hydrological model and remote sensing data are rather small, while those of ET products from GRACE through the water balance equation are large. As shown in black boxes in Figures 6(a) and 6(b), from long-term sequence interannual variations from 2003 to 2014, the upper reaches of YRB experienced a trough in 2006, which verifies the drought events in southwest China (the upper reaches of the Yangtze River) in 2006; however, the land hydrological model and remote sensing data do not detect this phenomenon. The parts marked out by black boxes in Figures 6(a) and 6(b) also show that the ET of each region shows distinct troughs, and in the middle reaches, it is different from that of high values in previous years but close to the mean annual ET of the other regions, which also monitors the drought events in the middle reaches of YRB in 2011. The land hydrological model and remote sensing data do not detect this phenomenon. Therefore, the ET estimation from GRACE through the water balance equation can monitor the drought events in YRB.

Seasonal variations of ET

YRB is controlled by the monsoon, especially in the middle and lower reaches, with four different seasons. It is of great significance to discuss deeply the seasonal variations of ET in different regions of the YRB. In Figure 7, there are average ET values for 12 months from land hydrological models (CLM, Mosaic, Noah and VIC), GRACE with the water balance equation (TRMM, GPCC) from August 2002 to August 2016 and MODIS products from August 2002 to December 2014.

According to Figure 7, the values of various ET products are close in each month, and the low values occur in January and December. From January in winter, to summer, the value of ET increases month by month, and then decreases from the high summer value to December in winter. However, there are differences between the results derived from the water balance equation and those from the land hydrological model and remote sensing data. There are two high values in the results from the water balance equation, namely, June and August in summer, while the rest of ET products have only one high value in July. In general, the values of 12 months' ET estimated from GRACE through the water balance equation are higher than those of products from the land hydrological model and remote sensing data.

Figure 8 shows the seasonal spatial distribution of ET, precipitation and surface temperature in the whole YRB, and the upper, middle and lower reaches. In these regions the spring includes March, April and May, the summer includes June, July and August, the autumn includes September, October and November, and the winter includes December, January and February.

Figure 8 a1, a2, a3 and a4 show the same pattern as Figure 7. In addition, the distribution of low values is shown in all regions in winter, and the distribution of high values is shown in all regions in summer (except for the

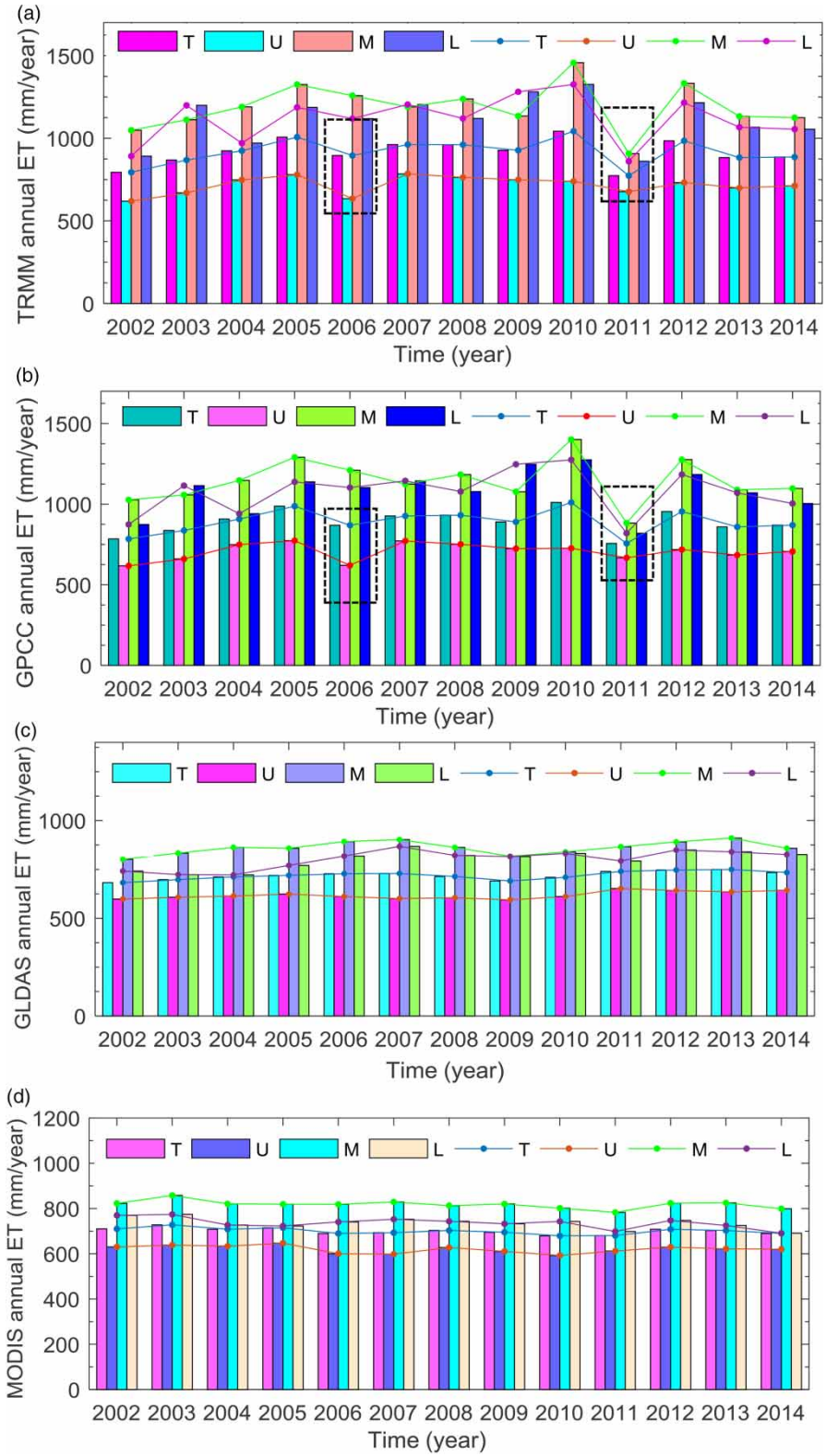

Figure 6 | Comparison of annual ET in the whole YRB (T), the upper reaches (U), the middle reaches (M) and the lower reaches (L) from 2002 to 2014.

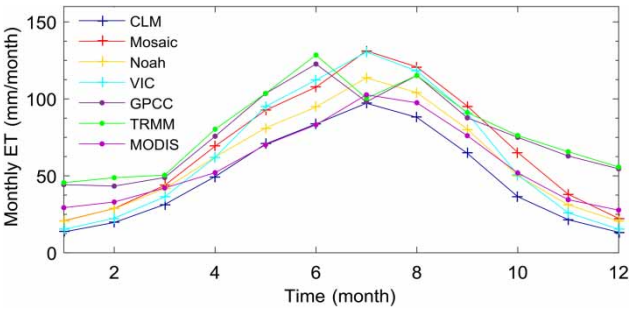

Figure 7 | Variations of average monthly ET in YRB.

low values in the upper reaches of the alpine regions in four seasons), while the distribution for the spring and autumn exhibits spatial diversity. As shown in Figure 8 a_1 and a_3, ET in the Three Gorges, Dongting Lake basin and Poyang Lake basin is higher, and the values of ET in Dongting Lake basin and Poyang Lake basin shown in Figure 8 a_1 are even closer to that of summer in Figure 8 a_3. Also the seasonal variation of ET is consistent with the spatial distribution of precipitation, especially in spring, and there is a remarkable consistency in the whole YRB between Figure 8 a_1 and Figure 8 b_1, which indicates that the precipitation is the main controlling factor of ET in spring. It also shows that ET in the southeast of middle reaches of the Yangtze River is significantly higher in Figure 8 a_1, which may be due to the monsoon land on the southeast coast in spring, resulting in more precipitation, and then the ET increases (Figure 8 a_1, b_1). In summer, although the precipitation in the upper reaches (Figure 8 b_2) is relatively high, ET in the upper reaches, especially in the alpine regions, does not rise. This can be seen from Figure 8 c_2: the surface temperature in the upper reaches in summer especially in alpine region is relatively low (except for the Sichuan basin with high temperature), leading to the result that ET does not increase with the increase of precipitation; and ET in the high temperature Sichuan basin is with higher values.

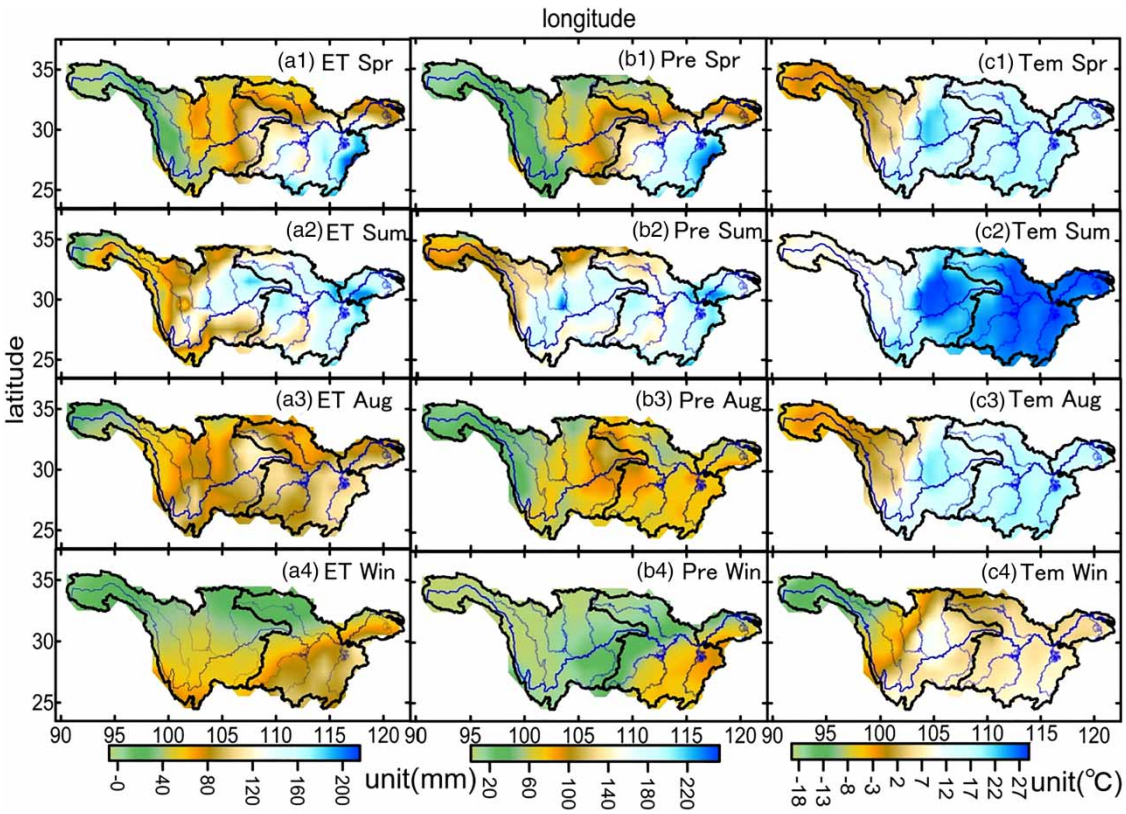

Figure 8 | Spatial distribution of the average ET, precipitation and temperature in the whole YRB, the upper, middle and lower reaches in four seasons from August 2002 to August 2016: a_1, a_2, a_3 and a_4 are respectively the ET derived from GRACE and TRMM in spring, autumn, summer and winter; b_1, b_2, b_3 and b_4 are respectively the precipitation from the GPCC model in spring, autumn, summer and winter; c_1, c_2, c_3 and c_4 are respectively the surface temperature from the GLDAS-Noah model in spring, autumn, summer and winter.

In other words, ET in the upper reaches of YRB is much more controlled by the surface temperature in summer.

Long-term variations of ET

The long-term variations are estimated through the fitting. Since ET shows significant trend, acceleration, seasonal variations with annual and semi-annual periods, it was fitted by Equation (2) with such terms, while 'sum of cos' is a summary of the annual term + semi-annual term. The long-term variations mean the trend at every 1×1 grid for the total YRB, so it is presented as a spatial distribution. The long-term variations of ET are respectively estimated by ET products from GRACE through the water balance equation (ET-$GRACE_{TRMM}$, ET-$GRACE_{GPCC}$), the land hydrological model (ET-$GLDAS_{Noah}$) and remote sensing data (ET-MODIS) from August 2002 to August 2016, which are shown in Figure 9. The variation velocities of the whole YRB, the upper, middle and lower reaches are calculated and shown in Table 1.

Figure 9 shows that the long-term variation trends of ET from GRACE through the water balance equation (ET-$GRACE_{TRMM}$, ET-$GRACE_{GPCC}$), the land hydrological model (ET-$GLDAS_{Noah}$) and remote sensing data (ET-MODIS) are consistent. Among them, the long-term variations of ET-$GRACE_{TRMM}$ and ET-$GRACE_{GPCC}$ are basically the same. Compared with ET-MODIS and ET-$GLDAS_{Noah}$, the spatial heterogeneity of ET-GRACE is larger, and slightly larger than ET-$GLDAS_{Noah}$. The trends of ET-$GRACE_{TRMM}$ and ET-$GRACE_{GPCC}$ increase significantly in the southeast of middle reaches and lower reaches of the YRB, reaching over 3.5 mm/yr. The Jianghan Plain and Dongting Lake basin in the middle reaches (about −0.5–0 mm/yr) and the alpine region in the upper reaches (varying in the range 0–0.5 mm/yr) show a consistent law of long-term variations in each ET product.

The values in Table 1 are the average of the long-term variations for the total upper, middle and lower basin respectively. According to Table 1, there are differences in long-term variations in various regions of YRB, and long-term variations of each ET product in the lower reaches are consistent, with the largest values, 0.98 mm/yr for ET-$GRACE_{TRMM}$, 1.14 mm/yr for ET-$GRACE_{GPCC}$ and 1.09 mm/yr for ET-$GLDAS_{Noah}$. However, the long-term variations of ET-MODIS are significantly lower in each region, but it also shows the most drastic variation in the lower reaches, with a value of

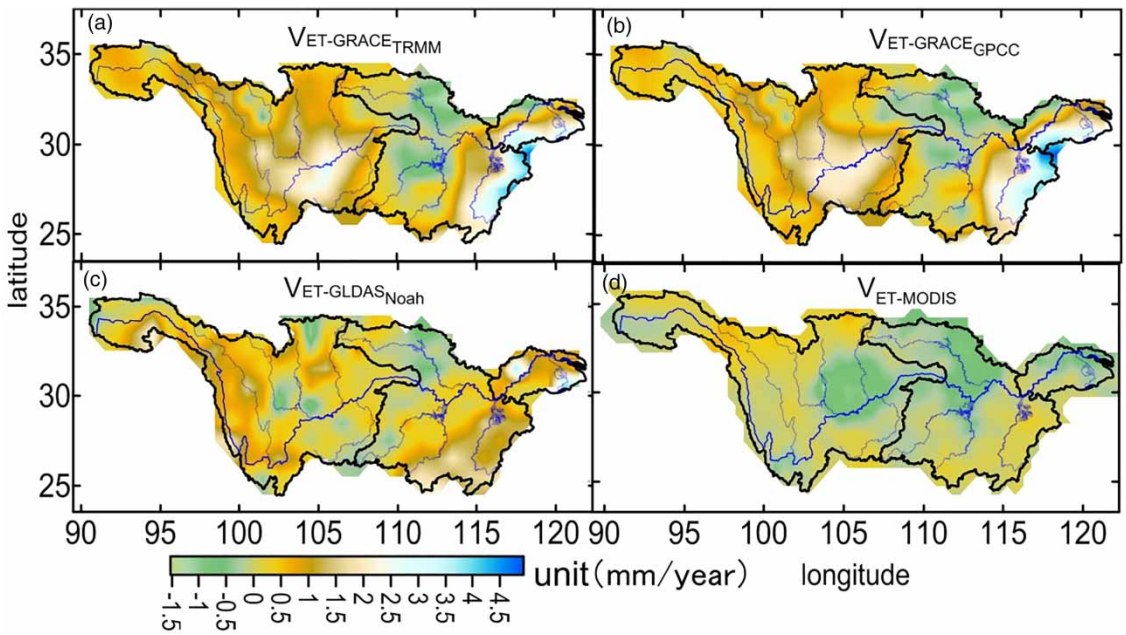

Figure 9 | Spatial distribution of the ET long-term variation trends in the whole, the upper, middle and lower reaches of YRB from August 2002 to August 2016: (a) variation velocities of ET from GRACE-TRMM, (b) variation velocities of ET from GRACE-GPCC, (c) variation velocities of ET from GLDAS, (d) variation velocities of ET from MODIS from August 2002 to November 2014.

Table 1 | Average variation trends of ET estimated from GRACE-TRMM, GRACE-GPCC and GLDAS in the whole YRB, the upper, middle and lower reaches from August 2002 to August 2016, and those of ET from MODIS from August 2002 to November 2014

Area \ mm/yr	$GRACE_{TRMM}$	$GRACE_{GPCC}$	$GLDAS_{Noah}$	MODIS
Total basin	0.79	0.75	0.48	− 0.12
Upper basin	0.79	0.72	0.38	− 0.08
Middle basin	0.74	0.72	0.52	− 0.16
Lower basin	0.98	1.14	1.09	− 0.23

−0.23 mm/yr. For long-term variations in the whole YRB, ET-$GRACE_{TRMM}$ is 0.79 mm/yr, ET-$GRACE_{GPCC}$ 0.75 mm/yr, ET-$GLDAS_{Noah}$ 0.48 mm/yr and ET-MODIS −0.12 mm/yr.

Influence factors of ET in YRB

Precipitation

From the above results and analysis, we find that the precipitation has a great impact on ET in YRB. The values of ET-GRACE and precipitation data from GPCC in each region of YRB were fitted in a long-term sequence and their correlation coefficients and variances were analysed; these are shown in Figure 10 and Table 2.

As can be seen from Figure 10, the precipitation and ET in YRB are in the same order of magnitude, and have the same seasonal variation trend with similar amplitude. However, Figure 10(b) shows that the amplitude of precipitation in the upper reaches is greater than that of ET, which indicates that the values of ET do not increase dramatically when the precipitation increases significantly. There are some qualifications, and the relative values are affected by ground conditions.

According to Table 2, each ET product has a great correlation with the precipitation, and the correlation coefficients are more than 0.71. Among them, the correlation coefficients of ET products from the land hydrological model are close to 1, which may be due to the fact that the input data of the land hydrological model contain precipitation data. The correlation between ET from the water balance equation and precipitation is of greater reference significance. Combining Figure 10 and Table 2, we can find that ET in the upper reaches is less affected by precipitation, but the precipitation is the dominant factor on ET in the middle and lower reaches

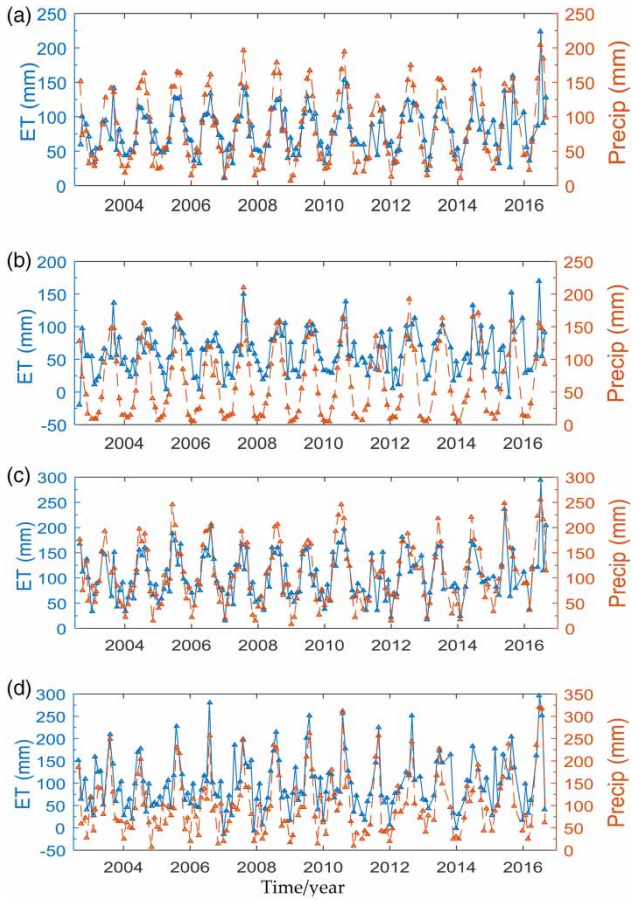

Figure 10 | Comparison of ET estimated from GRACE-TRMM model and precipitation data from GPCC in each region of YRB: (a) total YRB, (b) upper YRB, (c) middle YRB, (d) lower YRB.

Table 2 | Correlation coefficients (*r*) between ET and precipitation in each region of YRB

Precip	Total *r*	Upper *r*	Middle *r*	Lower *r*
ET_{TRMM}	0.85	0.78	0.84	0.86
ET_{GPCC}	0.84	0.77	0.83	0.86
$ET_{Gldas\text{-}vic}$	0.93	0.95	0.74	0.68
$ET_{Gldas\text{-}Noah}$	0.92	0.94	0.74	0.66
$ET_{Gldas\text{-}Mosaic}$	0.90	0.95	0.66	0.63
$ET_{Gldas\text{-}CLM}$	0.95	0.97	0.82	0.78
ET_{MODIS}	0.92	0.96	0.71	0.73

where the precipitation is higher with the correlation coefficients of $r = 0.84$ and $r = 0.86$, respectively. The correlation coefficient of the upper reaches is slightly smaller, with $r =$ 0.78, which also shows a great correlation.

Soil moisture

The soil moisture data were provided by GLDAS-Noah; four layers of soil in 0–2 meters were added. The values of ET-GRACE and soil moisture data in each region of YRB were fitted in a long-term sequence and their correlation coefficients and variances were analysed; these are shown in Figure 11 and Table 3. There is a large magnitude difference between ET and soil moisture in each region, the value of ET is about 100 mm/month, while the value of soil moisture is around 550 mm/month, but there is a certain correlation between them in long-term sequence variations (Figure 11).

Table 3 shows that the correlation coefficients between the values of each ET product and soil moisture in each region around 0.4, showing moderate correlations. All products show the highest correlation coefficient in the middle reaches with values reaching $r = 0.56$ and the lowest correlation coefficient in the upstream region with $r = 0.28$.

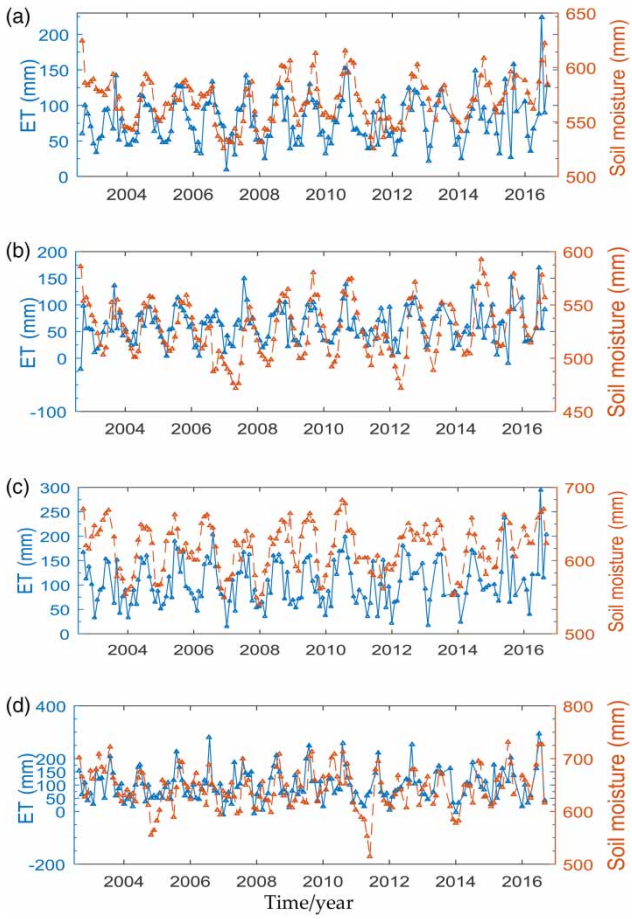

Figure 11 | Comparison of ET estimated from GRACE-TRMM model and soil moisture from GLDAS-Noah in each region of YRB: (a) total YRB, (b) upper YRB, (c) middle YRB, (d) lower YRB.

Table 3 | Correlation coefficients (*r*) between ET and soil moisture in each region of YRB

Soil moisture	Total *r*	Upper *r*	Middle *r*	Lower *r*
ET_{TRMM}	0.45	0.41	0.55	0.45
ET_{GPCC}	0.44	0.41	0.53	0.45
$ET_{Gldas\text{-}vic}$	0.50	0.28	0.49	0.37
$ET_{Gldas\text{-}Noah}$	0.49	0.30	0.50	0.40
$ET_{Gldas\text{-}Mosaic}$	0.49	0.33	0.40	0.31
$ET_{Gldas\text{-}CLM}$	0.50	0.29	0.56	0.50
ET_{MODIS}	0.53	0.34	0.48	0.50

Surface temperature

The surface temperature data were from the GLDAS-Noah model. The values of ET-GRACE and surface temperature data in each region of the YRB were fitted in a long-term sequence and their correlation coefficients and variances were analysed and are shown in Figure 12 and Table 4. According to Figure 12, the variation trends of surface temperature and ET are basically the same, but the variation of surface temperature is gentle, and they fit well in the summer high-value area (consistent with the analysis in 'Seasonal variations of ET'). The fluctuation of ET is greater, which may be due to the fact that ET is controlled by the coupling of various factors.

Table 4 shows the correlation coefficients of surface temperature and ET from the land hydrological model and remote sensing data are large, which is probably because the input data of the land hydrological model and remote sensing data include surface temperature data. The correlation between ET from the water balance equation and surface temperature is of greater reference significance. Comparing Table 4 with Table 3, we find that surface temperature has a great impact on ET, but the correlation coefficient (about 0.7) is slightly smaller than that of precipitation. Moreover, the correlation coefficient decreases progressively, i.e. upper > middle > lower.

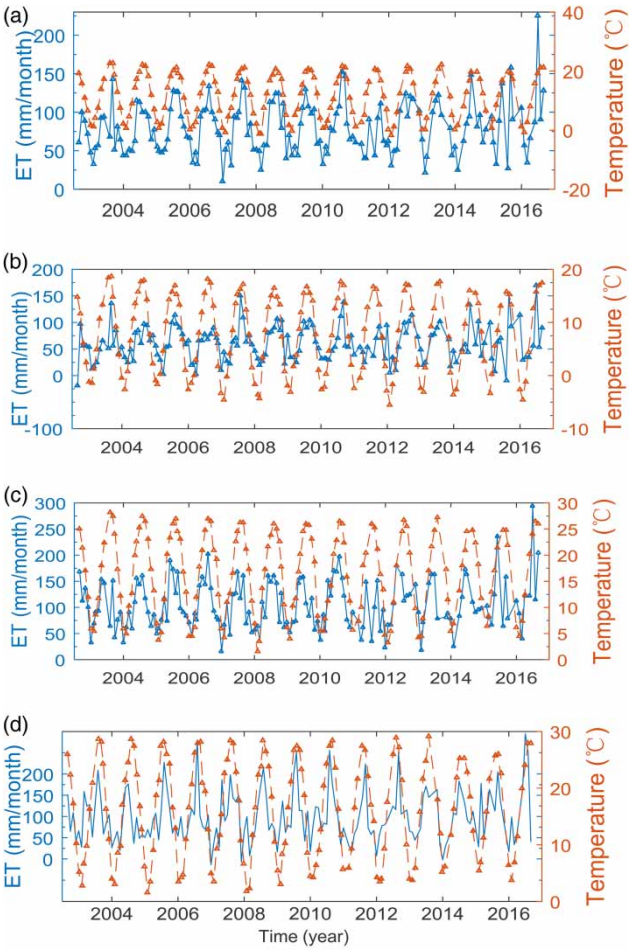

Figure 12 | Comparison of ET estimated from GRACE-TRMM model and surface temperature from GLDAS-Noah in each region of YRB: (a) total YRB, (b) upper YRB, (c) middle YRB, (d) lower YRB.

Table 4 | Correlation coefficients (*r*) between ET and surface temperature in each region

Temp	Total *r*	Upper *r*	Middle *r*	Lower *r*
ET_{TRMM}	0.84	0.77	0.69	0.61
ET_{GPCC}	0.84	0.70	0.71	0.61
$ET_{Gldas\text{-}vic}$	0.97	0.96	0.97	0.96
$ET_{Gldas\text{-}Noah}$	0.97	0.96	0.96	0.92
$ET_{Gldas\text{-}Mosaic}$	0.98	0.97	0.98	0.95
$ET_{Gldas\text{-}CLM}$	0.96	0.96	0.94	0.92
ET_{MODIS}	0.96	0.94	0.96	0.94

Solar radiation

The solar radiation data were used from GLDAS-Noah. The values of ET-GRACE and solar radiation data in each region of YRB were fitted in a long-term sequence and their correlation coefficients and variances were analysed and are shown in Figure 13 and Table 5. From Figure 13, the long-term sequence variation trend of solar radiation and ET in each region is basically the same and more consistent in the high-value area, while ET shows greater fluctuation in the low-value area, indicating that the surface ET is dominated by other factors rather than solar radiation when it is cloudy and rainy with low solar radiation.

According to Table 5, the correlation coefficients of solar radiation and ET from the land hydrological model and remote sensing data are large, which is probably because the input data of the land hydrological model and remote sensing data include solar radiation data.

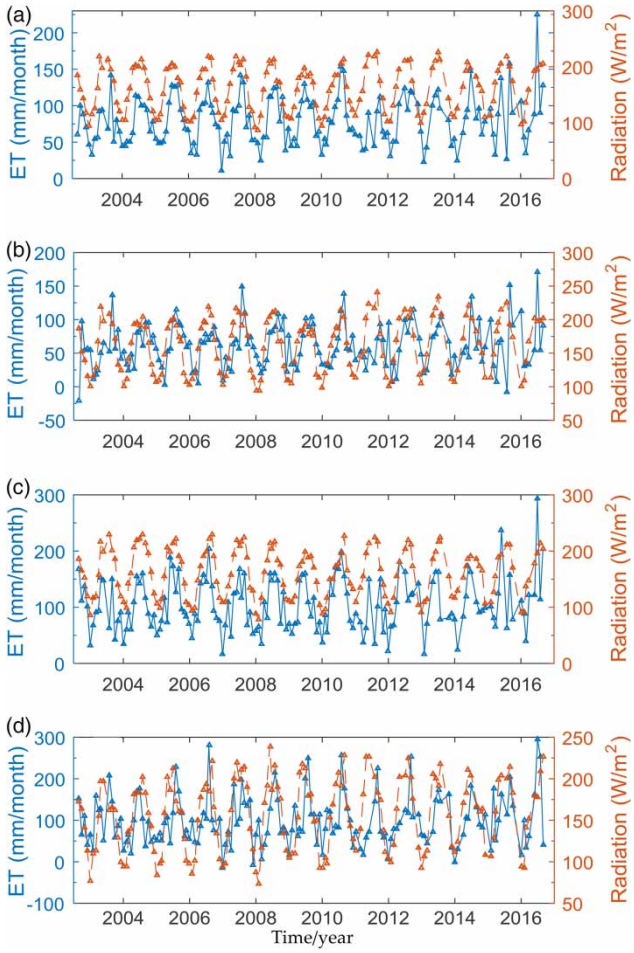

Figure 13 | Comparison of ET estimated from GRACE-TRMM model and solar shortwave radiation from GLDAS-Noah in each region of YRB: (a) total YRB, (b) upper YRB, (c) middle YRB, (d) lower YRB.

Table 5 | Correlation coefficients (*r*) of ET and solar shortwave radiation in each region of YRB

Solar radiation	Total *r*	Upper *r*	Middle *r*	Lower *r*
ET_{TRMM}	0.73	0.45	0.69	0.48
ET_{GPCC}	0.73	0.44	0.71	0.50
$ET_{Gldas\text{-}vic}$	0.90	0.85	0.94	0.84
$ET_{Gldas\text{-}Noah}$	0.91	0.84	0.96	0.94
$ET_{Gldas\text{-}Mosaic}$	0.90	0.83	0.94	0.93
$ET_{Gldas\text{-}CLM}$	0.91	0.83	0.93	0.85
ET_{MODIS}	0.85	0.77	0.90	0.76

Comparing Table 5 with Tables 2–4, the impact of solar radiation on ET is greater than soil moisture, slightly less than surface temperature, and much smaller than precipitation. The effect is different from the gradually descending law of surface temperature, with middle > lower > upper.

From the above influencing factors, we find that precipitation and temperature have the largest impact on the ET variations in whole YRB, and solar shortwave radiation, and soil moisture have a moderate impact. ET variations in the middle and lower YRB reaches are greatly affected by precipitation, and temperature plays a more important role in the upper YRB reaches, while the middle YRB reaches is mainly dominated by solar radiation.

DISCUSSION

In this study, the precipitation of TRMM data was converted from 0.25×0.25 grids to 1×1 grids. The effect on the estimation accuracy of conversion can be explained using a comparison. We also use GPCC as the precipitation in the water balance equation to calculate ET, and GPCC data is for a 1×1 grid. If ET-GRACE-TRMM is similar to ET-GRACE-GPCC, the accuracy of converting TRMM data will not be affected. Figure 2 shows us that ET-GRACE-TRMM is similar to ET-GRACE-GPCC. Furthermore, our GRACE-ET results are further validated by MODIS observations.

In addition, Figure 6 shows that GRACE-ET values reflect the drought events in 2006 and 2011. These two-year annual ET variations are much lower than other years from GRACE-ET, but the other products GLDAS-ET and MODIS-ET do not show anomalies. The drought events in 2006 and 2011 are historical events that were also validated by meteorological data. In addition, the ET in the YRB cannot be measured because the study area is too large to be measured by in-situ observations.

Figure 2 shows that in 2011 the GRACE-ET values were much lower than in other years, except for 2006. ET-GLDAS and ET-MODIS were not lower than usual in 2011. From the GRACE-ET in Figures 6(a) and 6(b), we see that in 2006, the drought event mainly happened in the upper basin of the YRB. The middle basin and lower basin annual ET values were high in 2006 which make up the loss of drought in the upper basin of the YRB leading to a normal ET value in the total basin. Therefore, it is not difficult to draw the conclusion that GRACE-ET had better performance than estimated ET by using other methods due to the higher ET values, but GRACE provides a new way to estimate ET variations.

Comparison of subgraphs in Figure 8 shows that ET in the Three Gorges area is high, no matter the distribution of precipitation and surface temperature, and regardless of seasons, which indicates that the construction of the Three Gorges Dam has increased the value of ET in the area. Perhaps the interception of the Three Gorges Dam increases the surface area of water, thus increasing the area of evaporation, or the construction of the dam reduces the vegetation coverage of the area, resulting in the weakening of vegetation effects on water retention, thereby increasing ET. In addition, other possible reasons include that the construction of the Three Gorges Dam has an impact on human water, irrigation and water storage.

Table 1 shows that the variation trends of ET-MODIS in each region are negative, which is not the same with other ET products (positive). This may be due to the different time range of data we adopt, i.e. MODIS data does not include 2015 and 2016.

CONCLUSIONS

Based on precipitation data provided by TRMM and GPCC, runoff data from GLDAS and GRACE data, ET in the whole YRB and its upper, middle and lower reaches was estimated by means of the water balance equation from August 2002 to

August 2016. The monthly average ET is compared with that of ET products from GLDAS and MODIS, showing good agreement. In addition, the interannual, seasonal, long-term variation and spatial distribution of ET in YRB were analysed in detail. Firstly, the values of 12 months' ET estimated from GRACE are higher than those of products from the land hydrological model and remote sensing data. Secondly, the GRACE data verify the severe drought events in 2006 and 2011. Thirdly, the influencing factors on ET variations in YRB were analysed.

The distribution of low values is shown in all regions in winter, and the distribution of high values is shown in all regions in summer (except for the low values in the upper reaches of the alpine regions in four seasons), while the distribution for the spring and autumn displays spatial diversity. ET in the Three Gorges, Dongting Lake basin and Poyang Lake basin is higher. The seasonal variation of ET is consistent with the spatial distribution of precipitation, especially in spring, which indicates that the precipitation is the main controlling factor for ET in spring. ET in the southeastern middle reaches of YRB is significantly higher because YRB is controlled by the monsoon, and the southwest monsoon lands on the southeast coast in spring, resulting in more precipitation, and then ET also increases. ET in the upper reaches of the Yangtze River is much more controlled by the surface temperature in summer.

Precipitation has the largest impact on ET ($r = 0.85$ for the whole YRB); surface temperature also has a great effect ($r = 0.84$ for the whole YRB), followed by solar shortwave radiation ($r = 0.73$ for the whole YRB), and soil moisture has a moderate impact ($r = 0.45$ for the whole YRB). ET in the middle and lower reaches of YRB is greatly affected by precipitation (values of r are 0.84 and 0.86 respectively); temperature has a more important role in the upper reaches ($r = 0.77$) and the middle reaches are controlled by solar radiation ($r = 0.71$).

ACKNOWLEDGEMENTS

The authors are grateful to those who made GRACE observations available. This research is supported by the National Natural Science Foundation of China (NSFC) Project (grant 11373059).

AUTHOR CONTRIBUTIONS

Xiaojuan Tian and Shuanggen Jin conceived and designed the experiments; Xiaojuan Tian performed the experiments and analysed the data as well as wrote the manuscript; Shunggen Jin revised and improved the manuscript. All authors contributed to the discussion of the results, as well as the writing of the manuscript.

CONFLICTS OF INTEREST

The authors declare no conflict of interest. The founding sponsors had no role in the design of the study; in the collection, analyses, or interpretation of data; in the writing of the manuscript, and in the decision to publish the results.

REFERENCES

Antonopoulos, V. & Antonopoulos, A. 2017 Daily reference evapotranspiration estimates by artificial neural networks technique and empirical equations using limited input climate variables. *Comput. Electron. Agric.* **132**, 86–96.

Bai, L. L., Cai, J., Liu, Y., Chen, H., Zhang, B. & Huang, L. 2017 Responses of field evapotranspiration to the changes of cropping pattern and groundwater depth in large irrigation district of Yellow River basin. *Agric. Water Manage.* **188**, 1–11.

Baik, J. & Choi, M. 2015 Evaluation of geostationary satellite (COMS) based Priestley–Taylor evapotranspiration. *Agric. Water Manage.* **159**, 77–91.

Hu, Z. Z. 1997 Interdecadal variability of summer climate over East Asia and its association with 500 hPa height and global sea surface temperature. *J. Geophys. Res.* **102** (D16), 19403–19412.

Jekeli, C. 1981 Alternative methods to smooth the Earth's gravity field. *Scientific Rep.* **327** (B12), 30205–30229. School of Earth Science: The Ohio State University.

Jin, S. G. & Feng, G. P. 2013 Large-scale variations of global groundwater from satellite gravimetry and hydrological models, 2002–2012. *Global Planet. Change* **106**, 20–30.

Jin, S. G. & Zou, F. 2015 Re-estimation of glacier mass loss in Greenland from GRACE with correction of land–ocean leakage effects. *Glob. Planet. Change* **135**, 170–178.

Jin, S. G., Zhang, L. & Tapley, B. 2011 The understanding of length-of-day variations from satellite gravity and laser ranging measurements. *Geophys. J. Int.* **184** (2), 651–660.

Jin, S. G., Tian, X. & Feng, G. 2016a Recent glacier changes in the Tien Shan observed by satellite gravity measurements. *Glob. Planet. Change* **143**, 81–87.

Jin, S. G., Zhang, T. & Zou, F. 2016b Glacial density and GIA in Alaska estimated from ICESat, GPS and GRACE measurements. *J. Geophys. Res. Earth Surface* **122**, 76–90.

Long, D., Yang, Y., Wada, Y., Hong, Y., Liang, W., Chen, Y., Yong, B., Hou, A., Wei, J. & Chen, L. 2015 Deriving scaling factors using a global hydrological model to restore GRACE total water storage changes for China's Yangtze River Basin. *Remote Sens. Environ.* **168**, 177–193.

Minacapilli, M., Agnese, C., Blanda, F., Cammalleri, C., Ciraolo, G., D'Urso, G., Iovino, M., Pumo, D., Provenzano, G. & Rallo, G. 2009 Estimation of actual evapotranspiration of Mediterranean perennial crops by means of remote-sensing based surface energy balance models. *Hydrol. Earth Syst. Sci.* **13** (7), 1061–1074. doi: 10.5194/hess-13-1061-2009.

Monteith, J. L. 1965 Evaporation and the environment. *Symp. Soc. Explor. Biol.* **19**, 205–234.

Najibi, N. & Jin, S. G. 2013 Physical reflectivity and polarization characteristics for snow and ice-covered surfaces interacting with GPS signals. *Remote Sens.* **5** (8), 4006–4030. doi: 10.3390/rs5084006.

Peltier, W. R. 2004 Global glacial isostasy and the surface of the ice-age earth: the ICE-5G 803 (VM2) model and GRACE. *Ann. Rev. Earth Planet. Sci.* **32**, 111–149.

Swenson, S. & Wahr, J. 2006 Post-processing removal of correlated errors in GRACE data. *Geophys. Res. Lett.* **33** (8), L08402.

Tapley, B. D., Bettadpur, S., Ries, J. C., Thompson, P. F. & Watkins, M. M. 2004 GRACE measurements of mass variability in the Earth system. *Science* **305**, 503–505.

Verstraeten, W. W., Veroustraete, F. & Feyen, J. 2008 Assessment of evapotranspiration and soil moisture content across different scales of observation. *Sensors* **8** (1), 70–117. http://dx.doi.org/10.3390/s8010070.

Wahr, J., Molennar, M. & Bryan, F. 1998 Time variability of the Earth's gravity field: hydrological and oceanic effects and their possible detection using GRACE. *J. Geophys. Res.* **103**, 205–230.

Wang, X., Huo, Z., Feng, S., Guo, P. & Guan, H. 2016 Estimating groundwater evapotranspiration from irrigated cropland incorporating root zone soil texture and moisture dynamics. *J. Hydrol.* **543**, 501–509.

Xu, Y., Xu, C., Gao, X. & Luo, Y. 2009 Projected changes in temperature and precipitation extremes over the Yangtze River Basin of China in the 21st century. *Quat. Int.* **208**, 44–52.

Yang, S. L., Liu, Z., Dai, S., Gao, Z., Zhang, J., Wang, H., Luo, X., Wu, C. & Zhang, Z. 2010 Temporal variations in water resources in the Yangtze River (Changjiang) over the Industrial Period based on reconstruction of missing monthly discharges. *Water Resource Res.* **46**, W10516. doi: 10.1029/2009WR008589.

Zhang, T. & Jin, S. G. 2016 Evapotranspiration variations in the Mississippi River Basin estimated from GPS observations. *IEEE Trans. Geosci. Remote Sens.* **54** (8), 4694–4701.

Zhang, Q., Xu, C.-Y., Zhang, Z., Chen, Y. D., Liu, C. & Lin, H. 2008 Spatial and temporal variability of precipitation maxima during 1960–2005 in the Yangtze River Basin and possible association with large-scale circulation. *J. Hydrol.* **353**, 215–227.

First received 11 April 2018; accepted in revised form 19 October 2018. Available online 26 November 2018